Journal of Applied Physics

Study of magnetocaloric effect and critical exponents in polycrystalline $La_{0.4}Pr_{0.3}Ba_{0.3}MnO_3$ compound

Cite as: J. Appl. Phys. **127**, 093902 (2020); https://doi.org/10.1063/1.5142337
Submitted: 12 December 2019 . Accepted: 17 February 2020 . Published Online: 05 March 2020

Dipak Mazumdar, Kalipada Das, and I. Das

Journal of Applied Physics ARTICLE scitation.org/journal/jap

Study of magnetocaloric effect and critical exponents in polycrystalline $La_{0.4}Pr_{0.3}Ba_{0.3}MnO_3$ compound

Cite as: J. Appl. Phys. **127**, 093902 (2020); doi: 10.1063/1.5142337
Submitted: 12 December 2019 · Accepted: 17 February 2020 ·
Published Online: 5 March 2020

Dipak Mazumdar,[1] Kalipada Das,[2,a)] and I. Das[1]

AFFILIATIONS

[1]Condensed Matter Physics Division, Saha Institute of Nuclear Physics, HBNI, 1/AF, Bidhannagar, Kolkata 700064, India
[2]Department of Physics, Seth Anandram Jaipuria College, 10 Raja Naba Krishna Street, Kolkata 700005, India

[a)]**Author to whom correspondence should be addressed:** kalipadadasphysics@gmail.com

ABSTRACT

Magnetic and magnetocaloric effects of the polycrystalline $La_{0.4}Pr_{0.3}Ba_{0.3}MnO_3$ (LPBMO) compound were extensively studied. The critical parameters were extracted from the magnetic isotherms data near the paramagnetic–ferromagnetic phase transition region. The values of the critical exponents were compared with the standard theoretically predicted universality classes of magnetism. Interestingly, the critical parameters exhibit anomalous nature compared to the standard models. Such a discrepancy was analyzed considering the effect of disorder present in the studied compound. Moreover, the material shows moderate values of the relative cooling power and refrigerant capacity. Additionally, we have also calculated the temperature-averaged entropy change and normalized refrigerant capacity for the studied LPBMO compound.

I. INTRODUCTION

In addition to the magnetic and magnetocaloric effects, critical exponent studies in doped perovskite manganites get utmost attention in recent years.[1–6] To explore the microscopic nature of the different types of magnetic interactions, the systematic study of the critical exponents gives a suitable direction to scientific study. Moreover, the existence and variation of the different competing interactions in doped perovskite manganites also make this branch suitable for the current research.[5,7–11] Doped perovskite manganite compounds are generally assigned by the general formula $RE_{1-x}B_xMnO_3$ (where RE is the trivalent ion and B is the bivalent ion). Depending upon the doping elements and concentration, the physical properties of the compound are greatly modified.[12–16] Some of the remarkable doping induced properties are charge ordering, metal insulator transition, ferromagnetism, colossal magnetoresistance (CMR),[17–19] large magnetocaloric effect (MCE), etc.[20] Among these, CMR and MCE studies have been widely performed due to their potential application as well as from the fundamental point of view.[21–25]

In the context of the magnetocaloric effect, it is defined as the isothermal entropy or adiabatic temperature change of any magnetic material in the presence of an external magnetic field. Nowadays, to replace the harmful gas compression cooling technology, the magnetocaloric effect study gets a prior commitment.[10,26–28] Due to the presence of some inherent interesting properties in manganite compounds like chemical stability, highly resistive, non-toxic, low price for production, etc., they carry a notable importance in the field of technological applications. On the other hand, if we concentrate on the fundamental aspects like construction of magnetic phase diagram, the magnetocaloric effect can be treated as a powerful tool to detect any feeble magnetic transition.[29–31] Magnetic and magnetocaloric properties of doped perovskite compounds are very much influenced by the local disorder parameter.[32–37] On the other hand, the critical exponents are very sensitive to the variation of the order parameter near the phase transition. Hence, it will be very interesting to study the magnetocaloric properties of doped perovskite manganite along with the critical exponents.

Extraction of the critical exponents only from the magnetocaloric effect by using magnetocaloric effect scaling laws as suggested by Franco *et al.* has been rarely investigated.[38–42] However, the critical exponents estimated from the magnetic isotherms using a set of power laws[43] in the vicinity of transition temperature, T_C, have been widely studied. It was reported in the literature about the unusual values of the critical exponents.[44–46] Additionally, it is worth mentioning that in case of the granular systems, strange

values of the critical exponents have been observed.[45] In this study, we have performed the magnetocaloric effect and critical exponents study for the polycrystalline $La_{0.4}Pr_{0.3}Ba_{0.3}MnO_3$ (LPBMO) compound. Previously, the disorder mediated magnetocaloric effect in the Ba-doped compound is reported by Rehman *et al.*[47] Considering this context, we have doped Pr-site by La-ions, and Ba doping concentration is reduced slightly to maintain the A-site cation radius as $Pr_{0.6}Ba_{0.4}MnO_3$. Moreover, very recently, Oumezzine *et al.* reported the magnetotransport and magnetic properties of the LPBMO sample having almost the same composition as the present studied compound. In addition to the second-order paramagnetic (PM) to ferromagnetic (FM) transition, the influence of the disorder on the physical properties is also described.[48]

Our study reveals that the critical exponents are very sensitive with the disorder induced by different A-site cationic radii. Additionally, the disorder induced large relative cooling power and refrigerant capacity of the polycrystalline LPBMO compound are also addressed.

II. SAMPLE PREPARATION, CHARACTERIZATIONS, AND MEASUREMENTS

To prepare polycrystalline $La_{0.4}Pr_{0.3}Ba_{0.3}MnO_3$ (LPBMO) compound by the well known solgel route,[49–52] we have used high purity (99.99%) La_2O_3, Pr_6O_{11}, $BaCO_3$, MnO_2, oxalic acid, nitric acid, and citric acid as precursors. All the rare-earth based oxides were preheated at 800°C for 12 h before use. Stoichiometric amounts of rare-earth oxides were converted into their corresponding nitrates form by adding concentrated nitric acid into the mixture and dissolving the solution into Millipore water. Due to the direct insoluble nature of MnO_2 in nitric acid, a required amount of oxalic acid was used to convert it to the oxalate form of the same nitrate solution. All the as prepared individual nitrate solutions of the constituent elements were mixed and magnetically stirred for 30 min to get a homogeneous mixture. A suitable amount of citric acid was added to the solution and the solution was allowed to set for evaporation slowly at 80 °C–90 °C in a water bath until the formation of the gel. Black porous powder was achieved by decomposing the gel at 200 °C. This black porous powder was then grounded, pelletized, and sintered at 1300 °C for 36 h to get the single phase polycrystalline LPBMO compound.

To check the phase purity and crystal structure, a room temperature x-ray diffraction (XRD) experiment has been performed in the powdered polycrystalline LPBMO compound by using a Cu-K_α source on the Rigaku-TTRAX-III diffractometer. Magnetization measurements have been carried out both in a super conducting quantum interference device (SQUID-VSM) and physical property measurement system (PPMS) (Quantum Design). We have used rectangular shape of the sample to avoid (minimizing) the demagnetization effect as reported earlier.[53,54]

III. EXPERIMENTAL RESULTS

A. X-ray diffraction analysis

The room temperature XRD spectra of the powdered LPBMO compound indicate that the compound was formed in single phase without any impurity phase. To gather more structural information about the compound, we have performed the Rietveld refinement (only profile fitting) of the XRD spectrum using FULLPROF software package. The theoretically simulated curve along with the experimental data points and Bragg positions have been shown in Fig. 1. The compound belongs to *Pnma* space group having an orthorhombic crystal structure. The refined lattice parameters are a = 5.860 Å, b = 5.526 Å, and c = 7.815 Å with a unit cell volume of 253.11 $Å^3$.

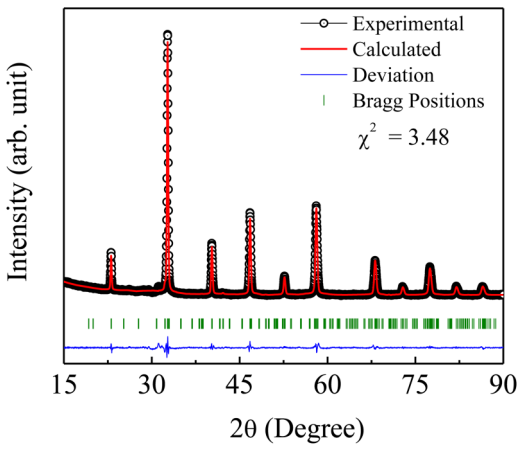

FIG. 1. Profile fitted x-ray diffraction spectrum of the powdered polycrystalline $La_{0.4}Pr_{0.3}Ba_{0.3}MnO_3$ compound measured at T = 300 K.

B. Magnetic properties

Magnetization as a function of an external magnetic field (M-H) in the protocol 0T ⟶ 7T ⟶ −7T ⟶ 7T at 5 K and 300 K has been performed as shown in Fig. 2(a). At 5 K, magnetization increases abruptly with an increase in very small magnetic field, and magnetization saturates completely with a saturation magnetization of 3.03 μ_B/f.u. The obtained saturation magnetization is less than that of the theoretically calculated value (4.66 μ_B/f.u.), and this may happen due to the presence of strong disorder in the system. At 5 K, a small hysteresis loop has been observed in the compound with coercive field, $H_C \sim 0.2$ kOe, and remanent magnetization, $M_r \sim 13$ emu/g, as shown in the inset of Fig. 2(a). Both very low saturation magnetic field and small hysteresis loss in the compound are advantageous from the technological application point of view. At 300 K, magnetization shows a non-linear dependence with the applied magnetic field specially at the low field region.

Temperature dependence of magnetization (M-T) measured in zero field cooled (ZFC) and field cooled (FC) protocols has been shown in Fig. 2(b). Low field (H = 500 Oe) temperature dependence of magnetization curve shows a bifurcation between ZFC and FC curves. This bifurcation may have arisen due to the presence of magnetic inhomogeneity, disorder, or multiple phases in the compound.[7,55] With decreasing temperature, magnetization increases continuously from a paramagnetic state to a ferromagnetic state and tends to saturate at very low temperatures. The magnetic transition

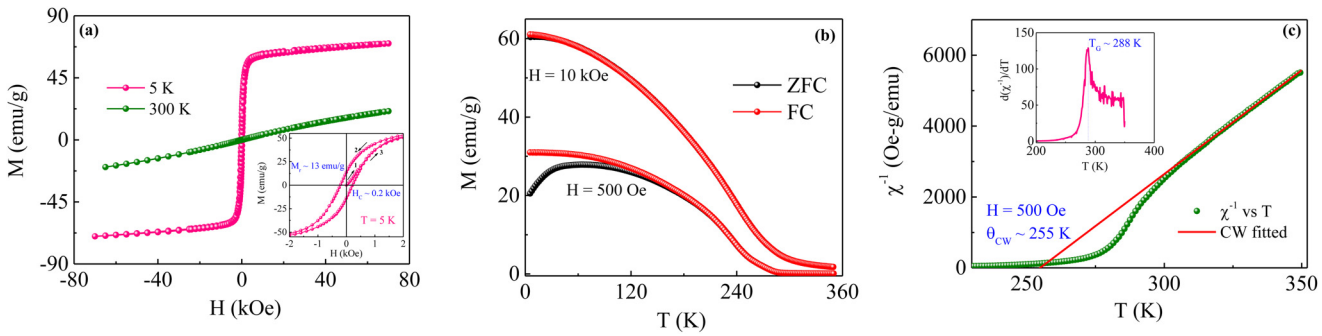

FIG. 2. (a) Magnetic field dependence of magnetization measured at T = 5 K and 300 K during the field sweeping 0 T → 7 T → −7 T → 7 T. The inset shows the zoomed portion of low field magnetization data for T = 5 K. (b) Variation of magnetization with respect to temperature measured at H = 500 Oe and 10 kOe. (c) The inverse susceptibility vs temperature plot along with the fitted Curie–Weiss law at high temperatures in a magnetic field of 500 Oe. The inset shows the presence of Griffiths phase in the compound from the $d\chi^{-1}/dT$ vs T plot.

temperature or Curie temperature (T_C) can be obtained from the minima of the temperature derivative of the FC-magnetization data, which is estimated to be ∼242 K. Upon application of 10 kOe external magnetic field, both ZFC and FC curves collapse with each other at low temperatures, indicating the transformation of mixed magnetic phase state into the FM one without any additional phase. There is no thermal hysteresis present between ZFC and FC curves, indicating the existence of continuous second-order phase transition (SOPT) in the vicinity of T_C.[56]

To understand the nature of high temperature paramagnetic state, inverse susceptibility as a function of temperature at H = 500 Oe has been plotted as shown in Fig. 2(c). Curie–Weiss (CW) law of the form $\chi = C/(T-\theta_{CW})$, where $C = \mu_{eff}^2/3k$ is the Curie constant and θ_{CW} stands for paramagnetic CW temperature, has been employed in the high temperature PM region of nonlinear χ^{-1} vs T plot. Therefore, the linear fitting of the χ^{-1} vs T curve gives a positive $\theta_{CW} \sim 255$ K. The positive value of Curie–Weiss constant clearly points the presence of ferromagnetic exchange interaction in the system.[3] The effective magnetic moment can be calculated theoretically by using the formula $(\mu_{eff})_{theo} = (0.3(\mu_{eff})^2_{Pr^{3+}} + 0.7(\mu_{eff})^2_{Mn^{3+}} + 0.3(\mu_{eff})^2_{Mn^{4+}})^{1/2}$, where $(\mu_{eff})_{Pr^{3+}}$, $(\mu_{eff})_{Mn^{3+}}$, and $(\mu_{eff})_{Mn^{4+}}$ are calculated with the help of $\mu_{eff} = g\sqrt{j(j+1)}\mu_B$ formula. The experimentally calculated effective magnetic moment $[(\mu_{eff})_{exp} = 5.73\,\mu_B$/f.u. for H = 500 Oe and $(\mu_{eff})_{exp} = 5.71\,\mu_B$/ f.u. for H = 10 kOe] from the slope of linearly fitted χ^{-1} vs T plot in the paramagnetic region is higher than that of the theoretically calculated value $[(\mu_{eff})_{theo} = 5.01\,\mu_B$/f.u.], which also indicates the presence of ferromagnetic clusters in the paramagnetic background.[18,57] This is basically due to the breaking of long-range ferromagnetic double exchange interaction by the induced quenched disorder in the system.[32] In addition to that, at low magnetic fields, χ^{-1} vs T plot exhibits the existence of the Griffiths phase in the studied compound as depicted in the inset of Fig. 2(c). Similar nature was also reported previously by Makni-Chakroun *et al.*[58] Oxygen deficiency in manganite compounds plays an important role in order to investigate its various physical properties. As reported earlier by Trukhanov *et al.*, the nature of the magnetic ground state drastically changes with the stoichiometry of the oxygen.[59] However, in our present studied compound, the nature of the magnetic ground state is similar to that of the reported compound.[33,48] Hence, it may be argued that oxygen stoichiometry does play the vital role in the present studied system.

C. Magnetocaloric effect (MCE)

In order to investigate the change of magnetic entropy (ΔS) of the studied LPBMO compound, a set of isothermal magnetization measurements have been carried out around a large temperature range of 30 K–350 K with an interval of 10 K with a field variation from 0 to 7 T as shown in Fig. 3(a). The compound exhibits ferromagnetic nature below T_C and reaches its saturation value with relatively very small magnetic field (<1 T) which is useful for MCE-based household applications.[20] With increasing temperature above T_C, ferromagnetism of the present compound tends to vanish, and almost a linear dependence of magnetization corresponds to the paramagnetic region has been achieved.

According to the classical Maxwell's thermodynamic relation,[60] the isothermal magnetic entropy changes is given by

$$\Delta S_M(T, H) = S_M(T, H) - S_M(T, 0) = \int_0^H (\partial M/\partial T)dH. \quad (1)$$

From the above equation, one can easily noticed that the change of magnetic entropy highly depends on the $(\partial M/\partial T)_H$ value. As a result, a huge change of magnetic entropy can be achieved in the vicinity of T_C. The magnetic entropy change (ΔS) as a function of temperature under various external magnetic fields have been shown in Fig. 3(b). The maximum value of −ΔS is 2.13 J/kg K for a field change of 0–7 T. Due to the shifting of effective Curie temperature, T_C by applied magnetic field, the peak value of −ΔS also moves toward higher temperature, which is clearly seen in case of our sample. Apart from the value of maximum entropy change ($-\Delta S_{max}$), ΔS vs T exhibits a significant broadening of temperature which is very useful from the technological perspectives. For a system which undergoes a second-order

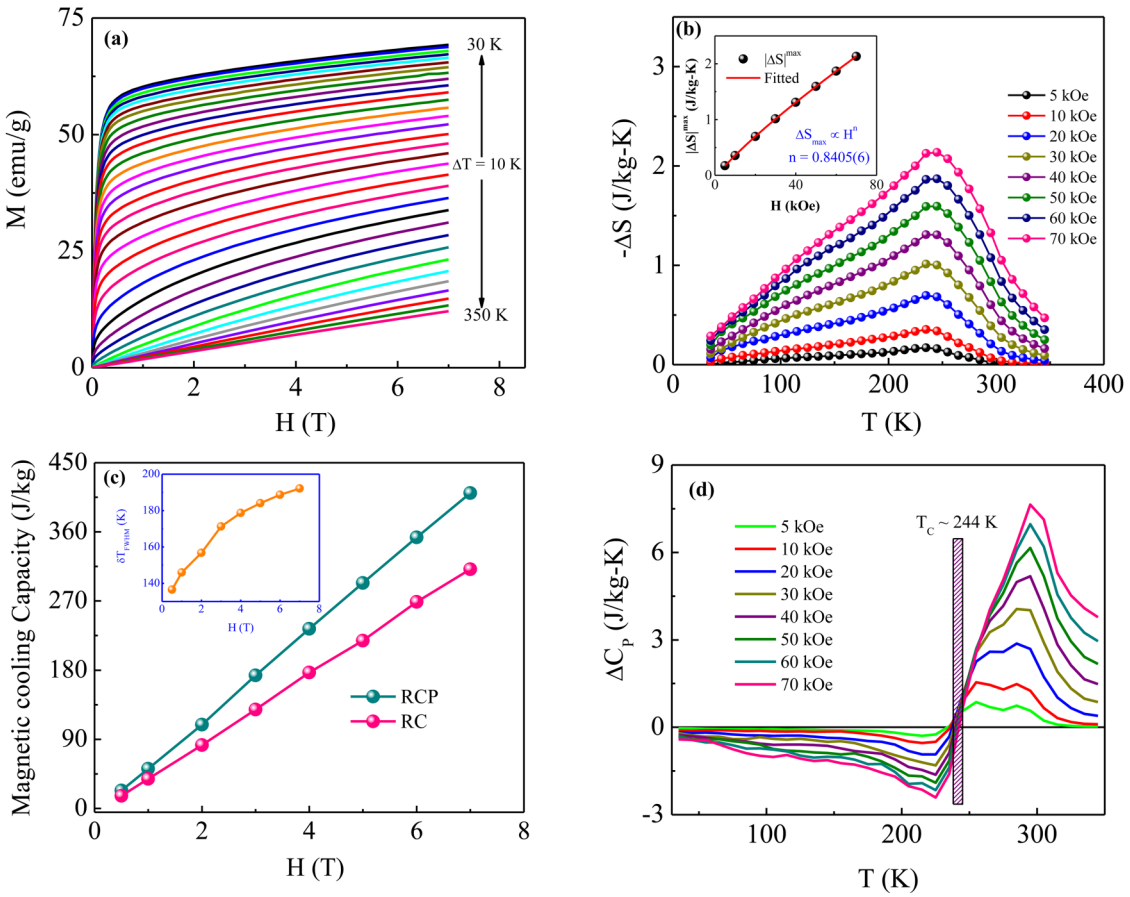

FIG. 3. (a) Isothermal magnetization as a function of applied magnetic field (M-H) measured at T = 30–350 K with an interval of 10 K. (b) Variation of isothermal magnetic entropy change (−ΔS) with respect to temperature calculated from the magnetization data. The inset shows the variation of $-\Delta S_{max}$ with the applied magnetic field along with the power law fitted curve. (c) Magnetic cooling capacity (both RCP and RC) as a function of applied magnetic fields. The inset shows the magnetic field dependence of δT_{FWHM}. (d) Temperature dependence of heat capacity change (ΔC_P) calculated for various applied magnetic fields.

magnetic phase transition, the variation of maximum value of entropy change ($-\Delta S_{max}$) with magnetic field follows a power law of the form $|\Delta S_{max}| \propto H^n$, where n is an exponent related to magnetic order of the system.[61,62] The variation of $|\Delta S_{max}|$ with H along with the power law fitted curve has been depicted in the inset of Fig. 3(b). The obtained value of n is about 0.8405, which is relatively higher than that of predicted by the mean-field model ($n = 0.6666$). This deviation in the value of n may have arisen due to the presence of local inhomogeneities or superparamagnetic clusters in the vicinity of the magnetic phase transition temperature existed in the present studied system.[63,64]

To determine the cooling capacity of a magnetic refrigerant material, a very significant parameter named magnetic cooling capacity[26,27] has been used. The net amount of heat transfer between a hot source and a cold sink in an ideal refrigeration cycle is coined as magnetic cooling capacity. Its value basically depends on the height and width of the −ΔS vs T curve. Different methods have been utilized to calculate the refrigerant capacity. The most simplest and popular method is the calculation of relative cooling power (RCP),[65] which is given as

$$RCP = |\Delta S|^{max} \times \partial T_{FWHM}, \tag{2}$$

where $|\Delta S|^{max}$ is the maximum value of entropy change and ∂T_{FWHM} is the full-width at half-maxima of the maximum entropy change at temperature scale.

Another method to estimate the magnetic cooling capacity[66] is given by the following relation:

$$RC = \int_{T1}^{T2} \Delta S dT, \tag{3}$$

where RC stands for the refrigerant capacity. Figure 3(c) shows the magnetic cooling capacity calculated in both ways as mentioned above as a function of applied magnetic field. The RCP value is significantly large (410 J/kg) for a field change of 7 T. Both RCP

and RC increase linearly with magnetic field due to the broadening of temperature. The broadening of temperature ∂T_{FWHM} is found to be increased with increasing applied magnetic field as shown in the inset of Fig. 3(c).

Both magnetic cooling capacities (RCP and RC) have been widely considered as ideal parameters for magnetic refrigerant materials. But these parameters are now known to be a misleading factor that overestimates the actual interest of a material for applications. In this occasion, temperature-averaged entropy change (TEC) has been suggested as a suitable and efficient figure-of-merit for the approximation of magnetocaloric properties of a magnetic refrigerant material.[67,68] For any magnetic refrigerant material, the TEC can be estimated with the help of isothermal entropy change $-\Delta S(T)$ by using the following equation:[68]

$$TEC = \frac{1}{\Delta T_{H-C}} \max\left\{\int_{T_{mid}-\frac{\Delta T_{H-C}}{2}}^{T_{mid}+\frac{\Delta T_{H-C}}{2}} |\Delta S(T)| dT\right\}, \tag{4}$$

where ΔT_{H-C} is the desired temperature span of the material which can easily give assistance to the response of magnetic field change ΔH.[67] Usually, ΔT_{H-C} is the temperature difference between the hot and cold heat exchangers ($\Delta T_{H-C} = T_{Hot} - T_{Cold}$) and T_{mid} is the temperature which maximizes the integration, i.e., TEC for the given value of ΔT_{H-C}. In our calculation process, we fixed the values of ΔT_{H-C} in between 5 K and 100 K with a step of 5 K and respective TEC is estimated for a magnetic field change of 5 T. The variation of TEC as a function of ΔT_{H-C} has been shown in Fig. 4. With the increasing values of ΔT_{H-C}, TEC gradually decreases. This kind of behavior was earlier reported by other research groups.[68–71]

Apart from TEC, another important figure of merit has been used to evaluate the performance of any magnetic refrigerant material is normalized refrigerant capacity (NRC).[68] This NRC is directly related to the already calculated refrigerant capacity (RC) as shown in Fig. 3(c) by adding an extra term $(1/H)$. We also calculated the NRC as a function of temperature difference between the hot and cold reservoirs ($\Delta T_{H-C} = T_{Hot} - T_{Cold}$) by using the following relation:

$$NRC = \frac{1}{H}\int_{T_{Cold}}^{T_{Hot}} |\Delta S| dT. \tag{5}$$

In this case also, we fixed the values of ΔT_{H-C} in between 5 and 100 K with a step of 5 K. NRC as a function of ΔT_{H-C} for a magnetic field change of 5 T has been shown in Fig. 4. The value of NRC increases with increasing the values of ΔT_{H-C}. This kind of behavior already seen in other caloric materials.[68,71,72]

The change of heat capacity $[\Delta C_P(T,H)]$ for a magnetic field variation from 0 to H is calculated[73] as

$$\Delta C_P(T, H) = C_P(T, H) - C_P(T, 0) = T\frac{\delta(\Delta S(T, H))}{\delta T}. \tag{6}$$

The calculated heat capacity change ΔC_P (T,H) as a function of temperature for various applied magnetic field has been shown in Fig. 3(d). A continuous change of sign of heat capacity data from negative to positive values around the transition temperature has been observed. This transition, in the vicinity of T_C, is accompanied by magnetic phase transition from ferromagnetic to paramagnetic state.[4] Moreover, values of ΔC_P (T,H) increase with increasing applied magnetic field. Regarding this context, it is worth mentioning that the total heat capacity is the combination of two parts below and above T_C, which generally affects the cooling or heating capacity of a magnetic refrigerant as reported by Zhang *et al.*[74]

In order to authenticate the nature of magnetic phase transition, Franco *et al.*[75–77] and Dong *et al.*[78] had proposed the construction of universal curve of magnetic entropy change. According to their proposal, the materials which undergo a second-order magnetic phase transition, all the normalized ΔS curves, should collapse into a single master curve irrespective of the external applied magnetic field by scaling the temperature axis. From experimental data, the universal curve may be extracted by normalizing all ΔS curves with respect to their peak value of entropy change as $\Delta S' = |\Delta S|/|\Delta S_{max}|$, and the temperature axis has to be rescaled by defining a parameter θ, above and below the transition temperature, T_C is expressed by the equation as

$$\theta = \frac{(T - T_C)}{(T_r - T_C)}, \tag{7}$$

where T_r is a reference temperature corresponding to a certain fraction "f" that satisfies $|\Delta S(T_r)|/|\Delta S(T_C)| = f$, as described earlier.[79] However, for inhomogeneous sample (magnetically) or small external magnetic field, two scaling parameters T_{r1} and T_{r2} (instead of T_r) have to be considered to remove the effect of demagnetization factor.[26,78,80] Therefore, the parameter θ is defined as

$$\theta = -\frac{(T - T_C)}{(T_{r1} - T_C)} \quad \text{for } T < T_C \tag{8}$$

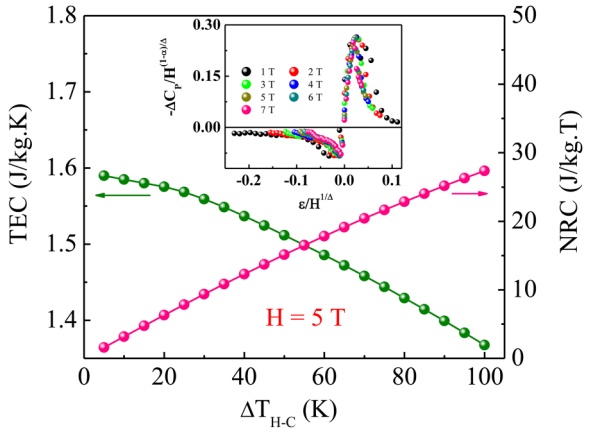

FIG. 4. Variation of temperature-averaged entropy change (TEC) and normalized refrigerant capacity (NRC) as a function of temperature difference between hot and cold reservoirs (ΔT_{H-C}). The inset shows the variation of scaled heat capacity with the scaled temperature which will be discussed in the last part of this section.

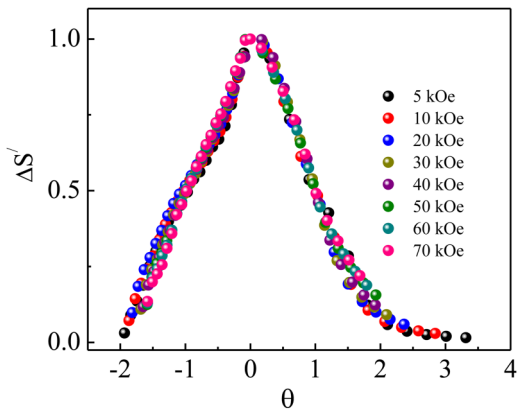

FIG. 5. Universal master curve: Variation of normalized entropy change ($\Delta S'$) as a function of rescaled temperature (θ) for different magnetic fields.

$$= 0 \quad \text{for } T = T_C \tag{9}$$

$$= \frac{(T - T_C)}{(T_{r2} - T_C)} \quad \text{for } T > T_C. \tag{10}$$

In this study, we have calculated the master curve by taking $f = 50$ % of maximum entropy change. The constructed curves according to the above scaling hypothesis for different applied magnetic fields are shown in Fig. 5. One can clearly see the collapses of all the data points into a single master curve irrespective of applied magnetic fields which confirms the presence of universal behavior associated with SOPT in the studied LPBMO compound.

D. Critical exponent analysis

To investigate the universality class in the present system, one has to calculate the critical exponents in the vicinity of magnetic phase transition temperature. For that purpose, a series of magnetic isotherms have been measured near the transition temperature, $T_C \sim 242$ K, which is shown in Fig. 6(a). With increasing temperature, magnetization decreases and it does not tend to saturate upon the application of 70 kOe magnetic field.

According to the mean-field theory, the magnetic equation of state[43,81] can be written as

$$\frac{H}{M} = a + bM^2, \tag{11}$$

where a and b are constants.[82] By using the procedure proposed by Banerjee *et al.* in the slope of H/M vs M^2 curve, one can identify the nature of magnetic phase transition. The slope is positive for a SOPT system and negative for a first-order phase transition (FOPT) system,[83] and the line passing through the origin is refereed as T_C. We have constructed the H/M vs M^2 curves (Arrott Plot)[81] as shown in Fig. 6(b), and all the curves show positive slopes with a non-linear behavior. Astonishingly, the line corresponding to T_C does not pass through the origin though the transition is second order in nature. So, to explore the values of critical exponents associated with LPBMO compound, we have analyzed the same magnetic isotherms with the help of modified Arrott plot (MAP) method known as Arrott–Noakes equation[84] of the state given by

$$\left(\frac{H}{M}\right)^{1/\gamma} = a\left(\frac{T - T_C}{T_C}\right) + bM^{1/\beta}, \tag{12}$$

where a and b are constants.

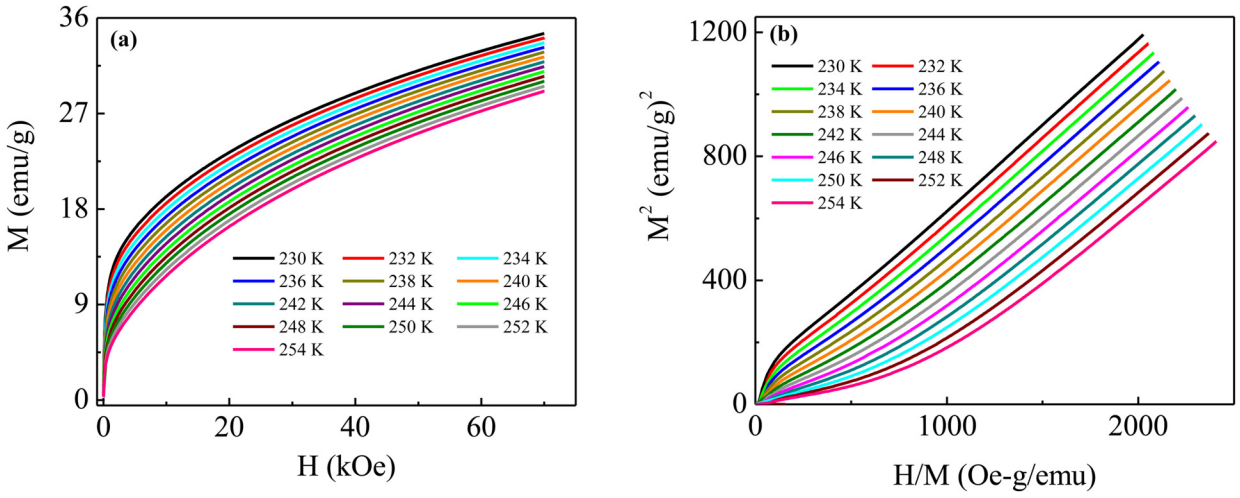

FIG. 6. (a) Isothermal magnetization (M-H) curves measured in the vicinity of T_C at various temperatures over the field range 0–7 T at 2 K interval. (b) Arrott plots (M^2—H/M) at different temperatures near T_C.

The critical exponents for a continuous magnetic phase transition near the Curie temperature, T_C, follow a set of power law dependence on the reduced temperature scale[43] which are described as

$$M_S(0, T) = M_S(-\varepsilon)^{\beta}, \quad \varepsilon < 0, \tag{13}$$

$$\chi_0^{-1}(0, T) = \left(\frac{H_0}{M_0}\right)(\varepsilon)^{\gamma}, \quad \varepsilon > 0, \tag{14}$$

$$M(H, T_C) = DH^{\frac{1}{\delta}}, \quad \varepsilon = 0, \tag{15}$$

where $\varepsilon = (T - T_c)/T_C$ is the reduced temperature and $M_S(0)$, H_0, and D are the critical amplitudes.

Besides the above scaling laws, these three critical exponents (β, γ, and δ) obey the Widom scaling relation[85] as given by

$$\delta = 1 + \frac{\gamma}{\beta}. \tag{16}$$

To further check the reliability and self-consistency of the critical exponents, magnetic equation of state derived from the scaling hypothesis has been used. According to the scaling hypothesis, the magnetic equation of state can be expressed as

$$M(H, \varepsilon) = |\varepsilon|^{\beta} f \pm \frac{H}{|\varepsilon|^{\beta+\gamma}}, \tag{17}$$

where f is a regular analytic function, f_+ for $T > T_C$, and f_- for $T < T_C$. Moreover, Eq. (17) can be rewritten in terms of renormalized magnetization $m \equiv |\varepsilon|^{-\beta} M(H, \varepsilon)$ and renormalized field $h \equiv |\varepsilon|^{-(\beta+\gamma)} H$ as

$$m = f \pm (h). \tag{18}$$

The above equation suggests that for the perfect values of β, γ, and ε, the m vs h curves will fall into two separate brunches of universal curves one for $T < T_C$ and the other for $T > T_C$.

By using the predicted critical exponents β and γ for various theoretical models given as the 3D Heisenberg model ($\beta = 0.365$, $\gamma = 1.386$),[5,86] 3D Ising model ($\beta = 0.325$, $\gamma = 1.241$),[5,86] 3D XY model ($\beta = 0.345$, $\gamma = 1.316$)[5,86], and tricritical mean-field model ($\beta = 0.25$, $\gamma = 1.0$),[87] MAPs have been constructed as shown in Fig. 7. All the models in the figure provide quasi-straight lines which are almost parallel to each other in the high magnetic field regions. Thus, it is not so easy to discriminate which one of them is the suitable one for determining the critical exponents. To find the best models for critical analysis, we have compared the relative slopes of the linearly fitted isotherms in the high field region. The relative slope, RS, defined as $RS = S(T)/S(T_C)$ and it is the degree of parallelism among the various $M^{1/\beta}$ vs $(H/M)^{1/\gamma}$ lines around T_C. The variation of RS with temperature is shown in Fig. 8(b). The most appropriate model is the one whose RS is close to unity above and below T_C, and corresponding β and γ values have been used as initial values for rigorous iteration to get the best version of the MAPs. From Fig. 8(b), it is clear that among all the models, the mean-field model deviates less than unity. Therefore, the initial parameters (β and γ) for MAPs were used as predicted for those of the mean-field model. Due to the suppression of the effect of charge, orbital, and lattice degree of freedom in the high field region, MAP has been constructed by taking the high field region data.

$M_S(0, T)$ and $\chi_0^{-1}(0, T)$ can be obtained by linear extrapolation of isotherms from the high field region to the intercepts of $M^{1/\beta}$ and $(H/M)^{1/\gamma}$ axes, respectively. The power laws of Eqs. (13) and (14) have been employed to the obtained temperature dependence of $M^{1/\beta}$ and $(H/M)^{1/\gamma}$ plot, yielding a new set of critical exponents β and γ, respectively. These values of β and γ are used for further iteration until their values become consistent and reliable. Using the values of $\beta = 0.694$ and $\gamma = 1.092$, a new MAP have been constructed as shown in Fig. 8(a). A set of parallel straight lines have been obtained and corresponding relative slopes of the isotherms have been calculated which is very close to 1 as shown in the same figure with other theoretically predicted models [Fig. 8(b)]. A straight line of the isotherms is passing through the origin which represent the critical temperature, $T_C = 244$ K. The presence of small curvature in the low field region of the isotherms in Fig. 8(a) may be due to the reorientation of magnetic domains at low magnetic fields.

Figure 9(a) shows the plots of the extracted values of $M_S(0, T)$ and $\chi_0^{-1}(0, T)$ as obtained from Fig. 8(a) and fitted the curves using the power laws of Eqs. (13) and (14). The non-linear fitting of $M_S(0, T)$ vs T plot yields $\beta = 0.666$ and $T_C = 244.01$ K and fitting of $\chi_0^{-1}(0, T)$ vs T plot gives $\gamma = 1.102$ and $T_C = 244.02$ K, which are almost close to the values of β and γ as obtained from MAPs.

To get a very effective and accurate values of the critical exponents as well as T_C, Kouvel–Fisher (KF) proposed[88] a method of linear dependence of $M_S(0, T)$ and $\chi_0^{-1}(0, T)$ with temperature by the analytical expression given as

$$\frac{M_S(T)}{dM_S(T)/dT} = \frac{T - T_C}{\beta}, \tag{19}$$

$$\frac{\chi_0^{-1}(T)}{d\chi_0^{-1}(T)/dT} = \frac{T - T_C}{\gamma}. \tag{20}$$

Equations (19) and (20) suggest that the $M_S(T)/[\partial M_S(0)/\partial T]$ vs T and $\chi_0^{-1}(T)/[d\chi_0^{-1}(T)/dT]$ vs T plot will generate two straight lines having slopes $1/\beta$ and $1/\gamma$, respectively, and upon linear extrapolation of these two straight lines intersect the temperature axis at the critical temperature T_C. The linear fitting of the plots following the KF method yields $\beta = 0.660(9)$ and $T_C = 243.85$ K and $\gamma = 1.091(8)$ and $T_C = 244.09$ K as shown in Fig. 9(b).

The third critical exponent δ can be obtained directly from the magnetic isotherm at $T = T_C$. From the linear fitting at high magnetic field of the M–H plot by using Eq. (15), a critical exponent $\delta = 2.566$ of the sample has been obtained and the corresponding fitting has been shown in the inset of Fig. 9(c). Widom scaling relation makes a bridge among the critical exponents as given by Eq. (16) and it has been utilized to crosscheck the reliability and self-consistency of the values of β and γ as obtained above. Table I represents a comparative visualization of all the critical exponents derived by various methods along with the theoretically predicted values for various models and already reported similar kinds of manganites. One can clearly see from Table I that the obtained values of the critical exponents for the present compound

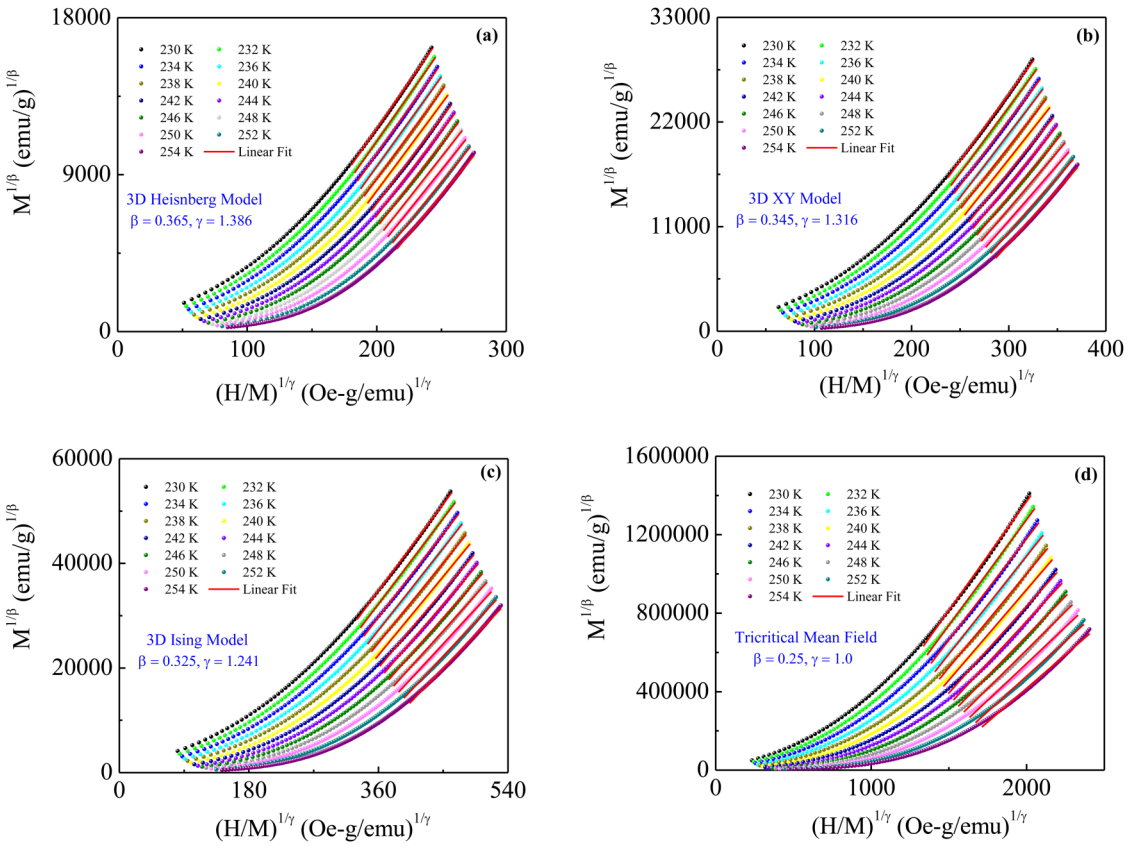

FIG. 7. Isothermal magnetization curves in the forms of modified Arrott plot [$M^{1/\beta}$ vs $(H/M)^{1/\gamma}$] in the temperature range of 230–254 K with an interval of 2 K for (a) 3D Heisenberg model, (b) 3D XY model, (c) 3D Ising model, and (d) tricritical mean-field model. Solid red lines are the linear fitted data in the high field region.

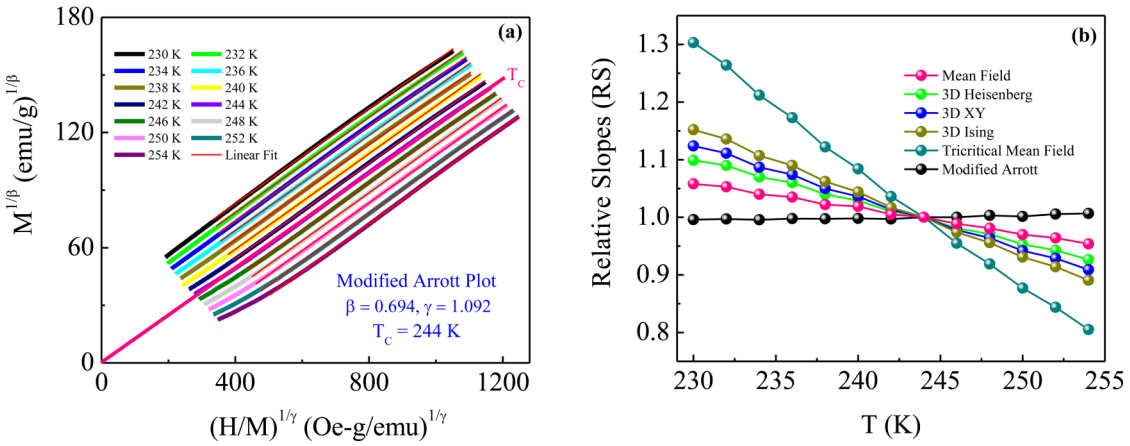

FIG. 8. (a) Modified Arrott plot [$M^{1/\beta}$ vs $(H/M)^{1/\gamma}$] of isotherms with $\beta = 0.694$ and $\gamma = 1.092$. The solid red lines are the linear fit of the isotherms at high field region. (b) Temperature dependence of relative slopes, RS = S(T)/S(T_C) in the vicinity of T_C.

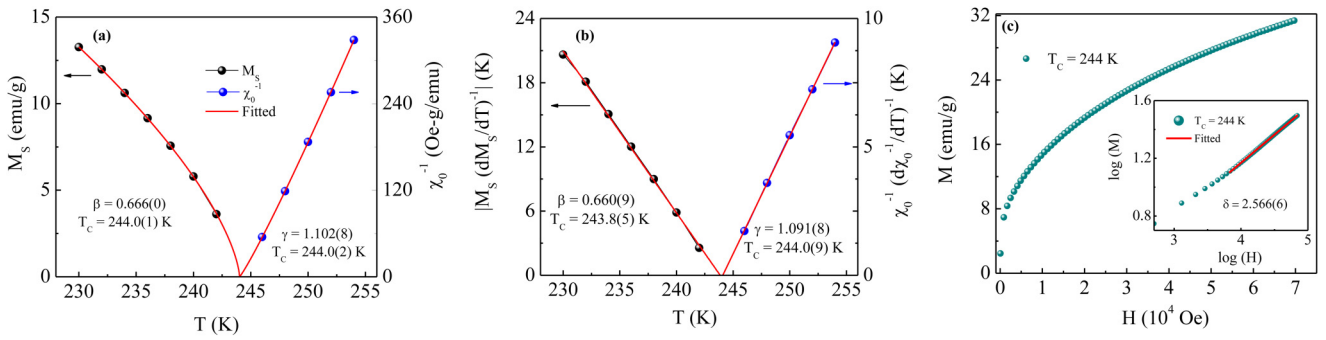

FIG. 9. (a) Temperature dependence of spontaneous magnetization [$M_S(0, T)$] and inverse initial susceptibility [$\chi_0^{-1}(0, T)$]. The solid red lines are the fit to the power law of Eqs. (13) and (14). (b) Kouvel–Fisher plots of $M_S(T)/[\partial M_S(0)/\partial T]$ vs T in the left and $\chi_0^{-1}(T)/[d\chi_0^{-1}(T)/dT]$ vs T in the right along with the linearly fitted red lines. (c) Field dependence of magnetization measured at $T_C = 244$ K. The inset shows the same data points in log–log scale along with the linearly fitted solid red line in the high field region obtained by using Eq. (15) to estimate the value of critical exponent δ from the inverse of the slope.

have no similarity with any one of the common universality classes. Therefore, it is necessary to justify whether these set of critical exponents can generate the scaling equation of state as given by Eq. (17). With the values of β, γ, and T_C as obtained from KF plot, we plotted $M|\varepsilon|^{-\beta}$ vs $H|\varepsilon|^{-(\beta+\gamma)}$ curves as shown in Fig. 10(a). The inset shows the same plot in the log–log scale to enlarge the low field region. It is proved from Fig. 10(a) that the obtained values of critical exponents β and γ are unambiguous and reasonably trustworthy as all the isotherms collapse onto two different brunches above and below the critical temperature, T_C. The self-consistency of the values of β, γ, and T_C are accurately further verified by constructing m^2 vs h/m curves as shown in Fig. 10(b). Again, all the curves fall onto two separate bunches: one above T_C and another below T_C. This clearly signifies that the interaction get properly renormalsized in a critical regime which follow both the scaling hypothesis and scaling equation of state.

Moreover, we have also calculated the effective values of the critical exponent given by the following relations:[89]

$$\beta_{eff} = \frac{d[\ln M_S(\varepsilon)]}{d(\ln \varepsilon)} \tag{21}$$

$$\gamma_{eff} = \frac{d[\ln \chi_0^{-1}(\varepsilon)]}{d(\ln \varepsilon)} \tag{22}$$

The calculated values of β_{eff} and γ_{eff} are almost unchanged within the reduced temperature range as shown in Fig. 11 which again proves the accuracy, reliability, and self-consistency of the critical exponents in the studied compound.

To further confirm the validity of the obtained critical exponents and the scaled equation of state [Eq. (17)], the obtained heat

TABLE I. Comparison of critical exponents of $La_{0.7-x}Pr_xBa_{0.3}MnO_3$ compound with different values of "x" and with some other manganites along with different theoretical models. Abbreviations: MAP, Modified Arrott plot; PL, Power law dependence; KF, Kouvel–Fisher method; and CI, Critical isotherm.

Material, model	Method	T_C (K)	β	γ	δ	References
Mean field	…	…	0.5	1.0	3	43
3D Heisenberg	…	…	0.365	1.386	4.8	5 and 86
3D Ising	…	…	0.325	1.241	4.82	5 and 86
3D XY	…	…	0.345	1.316	4.81	5 and 86
Tricritical mean field	…	…	0.25	1.0	5.0	87
$La_{0.4}Pr_{0.3}Ba_{0.3}MnO_3$	MAP	244	0.694	1.092	2.672	Present work
	PL	244.01	0.666	1.102	2.655	Present work
	KF	243.85	0.660	1.091	2.652	Present work
	CI	244	…	…	2.566	Present work
$La_{0.7}Ba_{0.3}MnO_3$	…	339.63	0.357	1.341	4.756	33
$La_{0.6}Pr_{0.1}Ba_{0.3}MnO_3$	…	320.86	0.391	1.348	4.447	33
$La_{0.5}Pr_{0.2}Ba_{0.3}MnO_3$	…	304.05	0.491	1.006	3.048	33
$Pr_{0.67}Ba_{0.33}MnO_3$	…	188	0.366	1.375	4.743	99
$La_{0.67}Ba_{0.33}MnO_3$	…	306	0.356	1.120	4.155	36

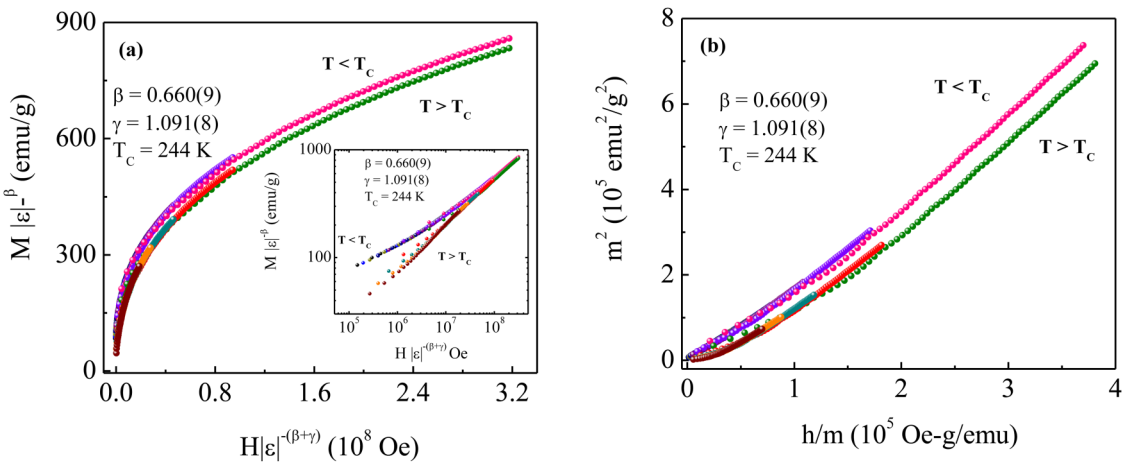

FIG. 10. (a) Scaling plot: Renormalized magnetization ($m \equiv M|\varepsilon|^{-\beta}$) as a function of renormalized field ($h \equiv H|\varepsilon|^{-(\beta+\gamma)}$) by using Eq. (17) with values of critical exponents obtained from the Kouvel–Fisher method. The inset shows the same plot in the log–log scale to expand the low magnetic field region. (b) Replotting of renormalized magnetization and magnetic field in the form of m^2–h/m above and below T_C.

capacity change (ΔC_P) can be written as[63,90]

$$\Delta C_P(T, H) = H^{(1-\alpha)/\Delta}[\varepsilon/H^{(1/\Delta)}], \tag{23}$$

where α is determined by using the Rushbrooke scaling relation:[90,91] $\alpha + 2\beta + \gamma = 2$ and $\Delta = \beta + \gamma$.[92] As a result, all the $-\Delta C_P/H^{(1-\alpha)/\Delta}$ vs $\varepsilon/H^{1/\Delta}$ curves should collapse onto a single master curve by using the generated critical exponents by various methods. In our investigation, we have used the critical exponents obtained from the Kouvel–Fisher method and plotted the $-\Delta C_P/H^{(1-\alpha)/\Delta}$ vs $\varepsilon/H^{1/\Delta}$ curves in the critical region as shown in the inset of Fig. 4. The merging of almost all the data points clearly points to the fact that the obtained values of β, γ, and T_C for this present LPBMO studied system are well in agreement with the scaling hypothesis.

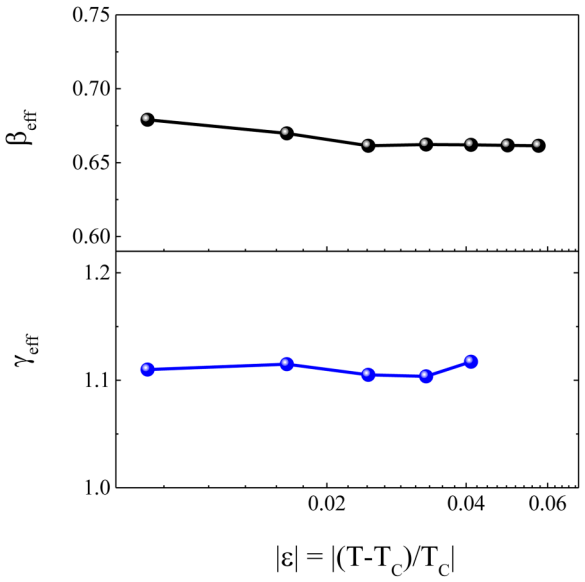

FIG. 11. Variation of effective values of critical exponents (β_{eff} for $T < T_C$ and γ_{eff} for $T > T_C$) as a function of reduced temperature $|\varepsilon| = |(T - T_c)/T_C|$ in the log–log scale.

IV. DISCUSSIONS

As mentioned earlier, the obtained critical exponents (β, γ, δ) do not belong to any theoretically predicted universality class although the value of γ is very close to that predicted for the mean-field theory. Therefore, the set of critical exponents obtained by various techniques for the studied sample is anomalous and the magnetic transition observed in the vicinity of T_C is unconventional. This kind of unconventional values of critical exponents was previously reported in the $La_{0.9}Pb_{0.1}MnO_3$ system where the presence of ferromagnetic cluster plays a vital role.[6] Furthermore, critical exponents are found to be almost abnormal in highly disorder systems.[33,93–95] This disorder basically arises due to the lattice mismatch of A-site or B-site ions as well as the nature of dopants and concentration, which significantly affect the values of critical exponents and transition temperature of a perovskite system.[44,93–95] Khelifi *et al.* had reported the critical behavior of polycrystalline $La_{0.7-x}Pr_xBa_{0.3}MnO_3$ ($x = 0$, 0.1, 0.2) compounds by varying the Pr^{3+} concentration and found an interesting result that with $x = 0$ and 0.1, the compound generally belongs to 3D Heisenberg Universality class and with $x = 0.2$, the compound has the β and γ values close to those predicted for the mean-field theory.[33] In the case of present compound $La_{0.4}Pr_{0.3}Ba_{0.3}MnO_3$, the value of γ is close to one. But the huge emergence of the value of β as compared to the mean-field theory rises some questions which one must need

to justify. As we mentioned earlier, the average A-site ionic radius, $\langle r_A \rangle$, with a constant fraction of Mn^{3+}/Mn^{4+} ratio can induce disorder in a system.[96,97] A-site disorder can be quantified by the relation $\sigma^2 = \sum x_i r_i^2 - \langle r_A \rangle^2$, where x_i is the fractional occupancies of the ith ion in the A-site.[34] The average A-site ionic radius $\langle r_A \rangle$ is directly proportional to the Mn–O–Mn bond angle, which favors the electronic conduction in manganite. With increasing values of $\langle r_A \rangle$ and its related quenched disorder σ^2, long-range ferromagnetic interaction strength becomes weaker and as a result, the transition temperature, T_C, decreases[3,35] as presented in Table II. The breaking of long-range order can create ferromagnetic clusters that may be surrounded by parramagnetic matrix and interaction converted into short-range type. As a result, the system can generate unexpected values of critical exponents which may be reliable and accurate too.

All the critical exponents have physical significance.[45] Basically, the critical exponents β describes the growth rate of the ordered magnetic moments. Higher values of β indicates a slower growth rate and vice versa. The exponent γ describes the nature of divergence of magnetic susceptibility at T_C. Smaller value of γ indicates the sharper divergence. The third critical exponent δ tells about the curvature of the critical isotherm. Large value of δ gives rapid saturation and vice versa. In the case of our system, β does not follow any model and has a higher value. The presence of huge quenched disorder in the present studied sample may resist the growth process of ferromagnetically ordered moments below the critical temperature, T_C, and as a result, we got an unexpected large value of β.

Another important decisive factor to understand the change of universality class along with quenched disorder of a system whose undergoes fully a second-order phase transition was proposed by Harris, generally known as the Harris criterion.[98] Before understanding the Harris criterion, one have to know about the critical exponent α^{pure}, which basically describes the divergence of the specific heat at the transition temperature, T_C. To check whether the obtained critical exponents in a pure system are stable or unstable against quenched disorder, the Harris criterion is widely used. According to the Harris criterion, the value of α^{pure} will be negative if the disorder is irrelevant and for relevant disorder, $\alpha^{pure} > 0$. The first condition ($\alpha^{pure} < 0$) is valid only for the system having short-range correlated quenched disorder or uncorrelated quenched disorder.[33] The specific heat exponent α^{pure} for our LPBMO system can be estimated by using the Rushbrooke scaling relation[90,91] given by $\alpha + 2\beta + \gamma = 2$. α^{pure} is negative in our case suggest that the disorder present in our sample is irrelevant, which helps us to justify the obtained critical exponents. Recently, Banik *et al.* showed that with the same average A-site ionic radius $\langle r_A \rangle$, the compounds $La_{0.7}Sr_{0.3}MnO_3$ ($\sigma^2 = 1.85 \times 10^{-3}$), $Pr_{0.7}Sr_{0.14}Ba_{0.16}MnO_3$ ($\sigma^2 = 1.17 \times 10^{-2}$), and $Nd_{0.7}Sr_{0.3}Ba_{0.23}MnO_3$ ($\sigma^2 = 1.66 \times 10^{-2}$) exhibit different universality classes, viz., the mean-field model, the tricritical mean-field model, and the 3D Heisenberg model, respectively.[3] This proves that quenched disorder of a pure system can easily tune its physical properties like critical temperature and the peak value of effective exponents along with the universality class to which the compound belongs.

TABLE II. Variation of Curie temperature (T_C), with average A-site ionic radius ($\langle r_A \rangle$), disorder parameter (σ^2), and Goldsmith Tolerance factor (t) of $La_{0.7-x}Pr_xBa_{0.3}MnO_3$ ($0 \le x \le 3$) along with other manganites.

Sample	$\langle r_A \rangle$ (Å)	σ^2 $\times 10^{-3}$	t	T_C (K)	References
$La_{0.7}Ba_{0.3}MnO_3$	1.292	13.54	0.952	339	33
$La_{0.6}Pr_{0.1}Ba_{0.3}MnO_3$	1.288	14.23	0.951	321	33
$La_{0.5}Pr_{0.2}Ba_{0.3}MnO_3$	1.284	14.89	0.950	304	33
$La_{0.4}Pr_{0.3}Ba_{0.3}MnO_3$	1.281	15.52	0.948	244	Present work
$Pr_{0.67}Ba_{0.33}MnO_3$	1.275	18.72	0.948	188	99
$Pr_{0.6}Ba_{0.4}MnO_3$	1.295	20.32	0.959	195	47

V. CONCLUSIONS

To summarize, we have carried out a detailed study of magnetic and magnetocaloric properties of $La_{0.4}Pr_{0.3}Ba_{0.3}MnO_3$ polycrystalline compound prepared by a standard solgel method. Our study indicates that a continuous paramagnetic to ferromagnetic phase transformation takes place at $T_C = 244$ K. The magnetocaloric entropy change exhibits a maximum value near the phase transition temperature. In addition to that, the critical exponents, in the vicinity of Curie temperature, were extracted by using various traditional techniques (from magnetic isotherms data). Astonishingly, our results indicate that the anomalous nature of the critical exponents does not belong to any theoretically predicted universality class. Such a distinguished nature of the critical exponents was addressed by employing the disorder effect in this compound.

ACKNOWLEDGMENTS

This work was supported by the Department of Atomic Energy (DAE), Government of India. The authors would like to thank S. Banik and N. Khan for fruitful discussions.

REFERENCES

[1]K. Ghosh, C. J. Lobb, R. L. Greene, S. G. Karabashev, D. A. Shulyatev, A. A. Arsenov, and Y. Mukovskii, Phys. Rev. Lett. **81**, 4740 (1998).
[2]M. Abassi, N. Dhahri, J. Dhahri, K. Tailbi, and E. K. Hlil, J. Rare Earths **33**, 263 (2015).
[3]S. Banik and I. Das, J. Alloy Comp. **742**, 248 (2018).
[4]R. M'nassri, Bull. Mater. Sci. **39**, 551 (2016).
[5]M. Camostrini, M. Hasenbusch, A. Pelissetto, P. Rossi, and E. Vicari, Phys. Rev. B **65**, 144520 (2002).
[6]T. L. Phan, S. G. Min, S. C. Yu, and S. K. Oh, J. Magn. Magn. Mater. **304**, 778 (2006).
[7]T. L. Phan, T. A. Ho, T. V. Manh, N. T. Dang, C. U. Jung, B. W. Lee, and T. D. Thanh, J. Appl. Phys. **118**, 143902 (2015).
[8]Y. Su, Y. Sui, J. G. Cheng, J. S. Zhou, X. Wang, Y. Wang, and J. B. Goodenough, Phys. Rev. B Condens. Matter Mater. Phys. **87**, 195102 (2013).
[9]A. Elhamza, S. E. L. Kossi, J. Dhahri, E. K. Hlil, M. A. Zaidi, and H. Belmabrouk, J. Magn. Magn. Mater. **460**, 480 (2018).
[10]A. M. Tishin and Y. I. Spichkin, *The Magnetocaloric Effect and Its Applications* (Institute of Physics Publishing, Bristol, 2003).
[11]N. A. de Oliveira and P. J. von Ranke, Phys. Rep. **489**, 89 (2010).

[12]Z. B. Guo, Y. W. Du, J. S. Zhu, H. Huang, W. P. Ding, and D. Feng, Phys. Rev. Lett. **78**, 1142 (1997).
[13]X. Bohigas, J. Tejada, E. delBarco, X. X. Zhang, and M. Sales, Appl. Phys. Lett. **73**, 390 (1998).
[14]Y. Sun, X. J. Xu, and Y. H. Zhang, J. Magn. Magn. Mater. **219**, 183 (2000).
[15]T. Tang, K. M. Gu, Q. Q. Cao, D. H. Wang, S. Y. Zhang, and Y. W. Du, J. Magn. Magn. Mater. **222**, 110 (2000).
[16]M. H. Phan, S. B. Tian, S. C. Yu, and A. N. Ulyanov, J. Magn. Magn. Mater. **256**, 306 (2003).
[17]K. Y. Wang, C. Sangregorio, J. Wiggins, J. Wiemann, and J. Tang, J. Appl. Phys. **87**, 5819 (2000).
[18]M. B. Salamon, P. Lin, and S. H. Chun, Phys. Rev. Lett. **88**, 197203 (2002).
[19]S. Banik, K. Das, T. Paramanik, N. P. Lalla, B. Satpati, K. Pradhan, and I. Das, NPG Asia Mater. **10**, 923 (2018).
[20]M. H. Phan and S. C. Yu, J. Magn. Magn. Mater. **308**, 325 (2007).
[21]M. Bibes and A. Bathelemy, IEEE Trans. Electron Devices **54**, 1003 (2007).
[22]A. Asamitsu, Y. Tomioka, H. Kuwahara, and Y. Tokura, Nature **388**, 50 (1997).
[23]D. Rubi, F. Tesler, I. Alposta, A. Kalstein, N. Ghenzi, F. Gomez-Marlasca, M. Rozenberg, and P. Levy, Appl. Phys. Lett. **103**, 163506 (2013).
[24]A. Sawa, Mater. Today **11**, 28 (2008).
[25]J. D. Hoffman, S. M. Wu, B. J. Kirby, and A. Bhattacharya, Phys. Rev. Appl. **9**, 044041 (2018).
[26]V. Franco, J. Blazquez, B. Ingale, and A. Conde, Annu. Rev. Mater. Res. **42**, 305 (2012).
[27]V. Franco, J. Blazquez, J. Ipus, J. Law, L. M. Ramirez, and A. Conde, Prog. Mater. Sci. **93**, 112 (2018).
[28]V. Franco and A. Conde, Int. J. Refrig. **33**, 465 (2010).
[29]K. Das, N. Banu, I. Das, and B. N. Dev, J. Magn. Magn. Mater. **487**, 165309 (2019).
[30]T. Paramanik, T. Samanta, R. Ranganathan, and I. Das, RSC Adv. **5**, 47860 (2015).
[31]D. Mazumdar, K. Das, S. Roy, and I. Das, J. Magn. Magn. Mater. **497**, 166066 (2020).
[32]K. F. Wang, Y. Wang, L. F. Wang, S. Dong, D. Li, Z. D. Zhang, H. Yu, Q. C. Li, and J.-M. Liu, Phys. Rev. B **73**, 134411 (2006).
[33]J. Khelifi, A. Tozri, E. Dhahri, and E. K. Hlil, J. Magn. Magn. Mater **349**, 149 (2014).
[34]L. M. Rodriguez-Martinez and J. P. Attfield, Phys. Rev. B **54**, R15622 (1996).
[35]J. Khelifi, A. Tozri, F. Issaoui, E. Dhahri, and E. K. Hlil, J. Alloy Comp. **584**, 617 (2014).
[36]N. Moutis, I. Panagiotopoulos, M. Pissas, and D. Niarchos, Phys. Rev. B **59**, 1129 (1999).
[37]F. Elleuds, M. Bekri, M. Hussain, M. Triki, E. Dhahri, E. K. Hlil, and L. Benais, Dalton Trans. **44**, 17712 (2015).
[38]V. Franco, A. Conde, J. M. Romero-Enrique, and J. S. Blazquez, J. Phys. Condens. Matter **20**, 285207 (2008).
[39]S. Dan, S. Mukherjee, C. Mazumdar, and R. Ranganathana, Phys. Chem. Chem. Phys. **21**, 2628 (2019).
[40]B. Mondal, S. Dan, S. Mondal, R. N. Bhowmik, R. Ranganathana, and C. Mazumdar, Phys. Chem. Chem. Phys. **21**, 16923 (2019).
[41]H. Omrani, M. Mansouri, W. C. Koubaa, M. Koubaa, and A. Cheikhrouhou, RSC Adv. **6**, 78017 (2016).
[42]J. Fan, X. Zhang, W. Zhang, D. Hu, Y. Zhu, Y. Shi, Y. Ying, L. Zhang, W. Tong, L. Pi, and Y. Zhang, Phase Transit. **87**, 676 (2014).
[43]H. Eugene Stanley, *Introduction to Phase Transition and Critical Phenomena* (Oxford University Press, New York, 1971).
[44]M. Triki, E. Dhahri, and E. K. Hlil, J. Solid State Chem. **201**, 63 (2013).
[45]F. Fang, B. Hong, L. Ling, J. Xu, H. Jin, D. Jin, X. Peng, J Li, Y. Yang, and X. Wang, RSC Adv. **6**, 22411 (2016).
[46]N. Tateiwa, Y. Haga, T. D. Matsuda, E. Yamamoto, and Z. Fisk, Phys. Rev. B **89**, 064420 (2014).
[47]Z. Ur Rehman, M. S. Anwar, and B. H. Koo, J. Supercond. Nov. Magn. **28**(5), 1629 (2014).
[48]M. Oumezzine, H. B. Sales, A. Selmi, and E. K. Hlil, RSC Adv. **9**, 25627 (2019).
[49]A. Biswas and I. Das, Phys. Rev. B **74**, 172405 (2006).
[50]A. Biswas, I. Das, and C. Majumdar, J. Appl. Phys. **98**, 124310 (2005).
[51]K. Das, P. Dasgupta, A. Poddar, and I. Das, Sci. Rep. **6**, 20351 (2016).
[52]K. Das, R. Rawat, B. Satpati, and I. Das, Appl. Phys. Lett. **103**, 202406 (2013).
[53]M. Das, S. Roy, and P. Mandal, Phys. Rev. B **96**, 174405 (2017).
[54]A. Midya and P. Mandal, J. Appl. Phys. **116**, 223905 (2014).
[55]D. N. H. Narn, R. Mathieu, P. Nordblad, N. V. Khiem, and N. X. Phuc, Phys. Rev. B **62**, 1027 (2000).
[56]O. Gutfleisch, T. Gottschall, M. Fries, D. Benke, I. Radulov, K. P. Skokov, H. Wende, M. Gruner, M. Acet, P. Entel, and M. Farle, Phil. Trans. R. Soc. A **374**, 20150308 (2016).
[57]M. M. Saber, M. Egilmez, A. I. Mansour, I. Fan, K. H. Chow, and J. Jung, Phys. Rev. B **82**, 172401 (2010).
[58]J. Makni-Chakroun, R. M'nassri, W. Cheikhrouhou-Koubaa, M. Koubaa, N. Chniba-Boudjada, and A. Cheikhrouhou, Chem. Phys. Lett. **707**, 61 (2018).
[59]S. V. Trukhanov, N. V. Kasper, I. O. Troyanchuk, M. Tovar, H. Szymczak, and K. Barner, J. Solid State Chem. **169**, 85 (2002).
[60]T. Hashimoto, T. Numasawa, M. Shino, and T. Okada, Cryogenics **21**, 647 (1981).
[61]H. Oesterreicher and F. T. Parker, J. Appl. Phys. **55**, 4334 (1984).
[62]S. Chandra, A. Biswas, S. Datta, B. Ghosh, V. Siruguri, A. K. Raychaudhuri, M. H. Phan, and H. Srikanth, J. Phys. Condens. Matter **24**, 366004 (2012).
[63]R. M'nassri, N. Chniba Boudjada, and A. Cheikhrouhou, J. Alloys Comp. **640**, 183 (2015).
[64]F. Saadaouia, R. M'nassri, H. Omrania, M. Koubaaa, N. Chniba Boudjada, and A. Cheikhrouhou, RSC Adv. **6**, 50968 (2016).
[65]V. K. Pecharsky and K. A. Gschneidner, J. Appl. Phys. **90**, 4614 (2001).
[66]S. Roy, M. Das, and P. Mandal, Phys. Rev. Mater. **2**, 064412 (2018).
[67]L. D. Griffith, Y. Mudryk, J. Slaughter, and V. K. Percharsky, J. Appl. Phys. **123**, 034902 (2018).
[68]S. Choura-Maatar, M. M. Nofal, R. M'nassri, W. C. Koubaa, N. C. Boudjada, and A. Cheikhrouhou, J. Mater. Sci. Mater. Electron. **31**, 1634 (2019).
[69]I. Hussain, S. N. Khan, T. N. Rao, and B. H. Koo, Ceram. Int. **45**, 16157 (2019).
[70]W. Zhong, W. Cheng, W. P. Ding, N. Zhang, Y. W. Du, and Q. J. Yan, Solid State Commun. **106**, 55 (1998).
[71]S. Mahjoub, R. M'nassri, M. Baazaoui, E. K. Hlil, and M. Oumezzine, J. Magn. Magn. Mater. **481**, 29 (2019).
[72]N. M. Bom, W. Imamura, E. O. Usuda, L. S. Paixao, and A. M. G. Carvalho, ACS Macro Lett. **7**, 31 (2018).
[73]A. Rostamnejadi, M. Venkatesan, P. Kameli, H. Salamati, and J. M. D. Coey, J. Magn. Magn. Mater. **323**, 2214 (2011).
[74]X. X. Zhang, G. H. Wen, F. W. Wang, W. H. Wang, C. H. Yu, and C. H. Wu, Appl. Phys. Lett. **77**, 3072 (2000).
[75]V. Franco, J. S. Blazquez, and A. Conde, Appl. Phys. Lett. **89**, 222512 (2006).
[76]V. Franco, R. Caballero-Flores, A. Conde, Q. Dong, and H. Zhang, J. Magn. Magn. Mater. **321**, 1115 (2009).
[77]V. Franco, A. Conde, V. Provenzano, and R. Shull, J. Magn. Magn. Mater. **322**, 218 (2010).
[78]Q. Y. Dong, H. W. Zhang, J. R. Sun, B. G. Shen, and V. Franco, J. Appl. Phys. **103**, 116101 (2008).
[79]A. Biswas, S. Chandra, T. Samanta, M. H. Phan, I. Das, and H. Srikanth, J. Appl. Phys. **113**, 17A902 (2013).
[80]C. R. Muniz, V. Franco, and A. Conde, Phys. Chem. Chem. Phys. **19**, 3582 (2017).
[81]A. Arrott, Phys. Rev. **108**, 1394 (1957).
[82]X. B. Liu and Z. Altounian, J. Magn. Magn. Mater. **292**, 83 (2005).
[83]S. K. Banerjee, Phys. Lett. **12**, 16 (1964).
[84]A. Arrott and J. Noakes, Phys. Rev. Lett. **19**, 786 (1967).
[85]B. Widom, J. Chem. Phys. **43**, 3898 (1965); *ibid.* **41**, 1633 (1964).

[86]J. C. Le Guillou and J. Zinn-Justin, Phys. Rev. B **21**, 3976 (1980).
[87]K. Huang, *Statistical Mechanics*, 2nd ed. (Wiley, New York, 1987).
[88]J. S. Kouvel and M. E. Fisher, Phys. Rev. **136**, A1626 (1964).
[89]N. Tateiwa, Y. Haga, and E. Yamamoto, Phys. Rev. B **99**, 094417 (2019).
[90]S. Tarhouni, R. M'nassri, A. Mleiki, W. Cheikhrouhou-Koubaa, A. Cheikhrouhoua, and E. K. Hlil, RSC Adv. **8**, 18294 (2018).
[91]J. J. Binney, N. J. Dowrick, A. J. Fisher, and M. E. J. Newman, *The Theory of Critical Phenomena* (Oxford University Press, Oxford, 1992).
[92]A. Hankey and H. E. Stanley, Phys. Rev. B **6**, 3515 (1972).
[93]T. L. Phan, T. A. Ho, P. D. Thang, Q. T. Tran, T. D. Thanh, N. X. Phuc, M. H. Phan, B. T. Huy, and S. C. Yu, J. Alloys Comp. **615**, 937 (2014).
[94]T. A. Ho, T. L. Phan, P. D. Thang, and S. C. Yu, J. Electron. Mater. **45**, 2328 (2016).
[95]D. Akahoshi, M. Uchida, Y. Tomioka, T. Arima, Y. Matsui, and Y. Tokura, Phys. Rev. Lett. **90**, 177203 (2003).
[96]Y. Moritomo, H. Kuwahara, Y. Tomioka, and Y. Tokura, Phys. Rev. B **55**, 7549 (1997).
[97]R. Mathieu, M. Uchida, Y. Kaneko, J. P. He, X. Z. Yu, R. Kumai, T. Arima, Y. Tomioka, A. Asamitsu, Y. Matsui, and Y. Tokura, Phys. Rev. B **74**, 20404 (2006).
[98]A. B. Harris, J. Phys. C Solid State Phys. **7**, 1671 (1974).
[99]A. Varvescu and I. G. Deac, Phys. B Condens. Matter. **470**, 96 (2015).